THE ASTROPHYSICAL JOURNAL, 425:195–204, 1994 April 10

THE ROLE OF THE EQUATION OF STATE IN THE "PROMPT" PHASE OF TYPE II SUPERNOVAE

F. DOUGLAS SWESTY,[1,2,3] JAMES M. LATTIMER,[2] AND ERIC S. MYRA[4]
Received 1993 May 19; accepted 1993 October 13

ABSTRACT

We examine the role of the equation of state (EOS) of hot, dense matter in the prompt phase of stellar collapse. In order to achieve this goal, we have carried out radiation hydrodynamic simulations using an adjustable EOS that is consistent with constraints placed on the EOS by neutron star observations, nuclear systematics, and laboratory experiments. Our simulations of stellar collapse show that these constraints restrict the role that the EOS can play in determining the dynamics of shock propagation. We find that certain nuclear force parameters do not substantially affect the dynamics of collapse as strongly as previously believed. In particular, we find that the shock stall radius is practically independent of the compression modulus and symmetry energy when other constaints on the EOS are satisfied. In contrast, the nuclear symmetry energies have more profound effects on the collapse via electron capture, and these effects may be detectable by means of the neutrino signature of a nearby supernova.

Subject headings: dense matter — equation of state — shock waves — stars: neutron — supernovae: general

1. INTRODUCTION

It has been suggested that the equation of state (EOS) of hot, dense matter may underlie the explosion mechanism of gravitational collapse supernovae. The usual assumption is that softer EOSs work in favor of the explosion mechanism. One of our goals in this paper is to explore this assumption and another is to explore the analogous question for the symmetry energy behavior of the EOS.

The role that the EOS of hot, dense matter plays in Type II supernovae has long been the subject of detailed numerical investigations. These investigations have largely been motivated by the fact that the behavior of matter at nuclear densities and above is not yet well constrained by experiment or observation. Yet the behavior of matter at high densities plays a critical role in both the dynamics of the "prompt" phase (the epoch encompassing the collapse and bounce of the iron core) as well as the subsequent evolution to later times.

Following the bounce of the core, when the density in the core exceeds nuclear density, a powerful shock wave is produced. At one time it was thought that this shock would propagate through the outer core regions and through the rest of the star, producing an explosion and a supernova. Although it is widely believed that this shock cannot, by itself, lead to an explosion, the existence of the shock is certainly necessary for all plausible explosion mechanisms. These include neutrino reheating that reenergizes the shock and convective overturn that rapidly transports energy into the region behind the shock. Moreover, the strength of the initial bounce and the structure of the post-bounce core are crucial to the operation of these "late-time" mechanisms. Thus, it is vital to understand how the uncertainties in the EOS will influence the collapse and bounce of the core.

One can characterize aspects of the EOS of matter at nuclear densities in terms of parameters which can, in theory, be constrained by laboratory measurements. In practice, however, a number of these parameters have proved very difficult to extract from experimental data. This is because the experiments are performed on finite-sized nuclei which do not span a large range of neutron excesses, densities, or sizes.

Three of the most interesting, and uncertain, parameters involve the incompressibility, symmetry energy coefficient, and the specific heat of bulk nuclear matter. These parameters can be expressed as second derivatives of the Helmholtz free energy per baryon, f, of bulk nuclear matter and are defined by

$$K_s = 9n_s^2 \left.\frac{\partial^2 f}{\partial n^2}\right|_{n=n_s, x=1/2, T=0}, \quad (1)$$

$$S_v = \frac{1}{8} \left.\frac{\partial^2 f}{\partial x^2}\right|_{n=n_s, x=1/2, T=0}, \quad (2)$$

and

$$a_v = -\frac{1}{2} \left.\frac{\partial^2 f}{\partial T^2}\right|_{n=n_s, x=1/2, T=0}, \quad (3)$$

where n_s is the saturation density of cold, symmetric nuclear matter, x is the proton fraction, and T is the temperature. Estimates of n_s lie in the relatively small range of 0.148–0.17 fm^{-3}. K_s is the bulk incompressibility, S_v is the bulk, or volume, symmetry energy coefficient, and a_v is the bulk specific heat of nuclear matter. As we show in § 3, other important EOS parameters are largely correlated to the values of K_s and S_v. The role of the level density parameter is largely muted by the dynamics of the collapse as we will discuss in § 5. For this reason, the role of the EOS in stellar collapse can be conveniently addressed by confining attention to the variation of K_s and S_v.

A number of studies have been conducted in an attempt to delineate the exact role of the EOS in the collapse and bounce phases of a Type II supernova (Baron, Cooperstein, & Kahana

[1] Department of Physics, State University of New York at Stony Brook, Stony Brook, NY 11794.
[2] Department of Earth and Space Sciences, State University of New York at Stony Brook, Stony Brook, NY 11794.
[3] Postal address: Laboratory for Computational Astrophysics, National Center for Supercomputer Applications, University of Illinois at Urbana-Champaign, 405 N. Mathews Avenue, Urbana, IL 61801.
[4] Intel Corporation, Supercomputer Systems Division, 14924 NW Greenbrier Parkway, Beaverton, OR 97006.

1985a, b [hereafter BCK]; Baron et al. 1987; Myra & Bludman 1989 [hereafter MB]; Bruenn 1989a, b; Cooperstein & Baron 1990; Miralles et al. 1991). Many of these investigations have been largely motivated by the observation that softening the EOS above nuclear densities in some cases results in stronger bounces and shocks. This was first indicated in a systematic study (Van Riper 1978) where it was found, using a polytropic EOS, that shock strength was directly correlated with EOS softness, up to the point where the collapse never halted and a black hole was formed (Van Riper 1979). BCK and Baron et al. (1987) used the Cooperstein & Baron (1990) EOS (hereafter referred to as the CB EOS), in which the incompressibility and adiabatic index of supernuclear matter were varied, and found this same general trend. Additionally, they claimed that sufficiently soft equations of state could be devised that could result in explosions before collapse to a black hole ensued. More series of confirming simulations were performed Myra & Bludman (1989) and by Bruenn (1989a, b) using the CB EOS. A constraint which all these studies have failed to address is that the maximum mass of a neutron star is at least 1.44 $M_\odot$ (Weisberg & Taylor 1984). Most of the aforementioned simulations have utilized equations of state that do not meet this requirement.

The relative softness of the EOS is not the only property that has been explored in supernovae simulations. The strength of supernovae shocks also strongly depends on the extent to which electron capture reactions deleptonize the core during the collapse epoch. A high rate of electron capture results in a smaller homologous core, which, in turn, results in a weaker shock (Lattimer, Burrows, & Yahil 1986). In addition, when the homologous core is smaller there is more of the outer iron core that the shock must transverse in order to escape. Since the primary work done by the shock is in dissociating nuclei, as the outer core size increases, so does the energy spent by the shock traveling through it. The extent of electron capture is primarily controlled by the nuclear symmetry energy, which can be conveniently expressed in terms of $\hat{\mu}$, the difference of neutron and proton chemical potentials. The electron capture rate varies directly with $\mu_e - \hat{\mu}$, so the larger $\hat{\mu}$ is, the smaller the consequent capture rate. Bruenn (1989a) also investigated the role of the nuclear symmetry energy and has found that decreasing $\hat{\mu}$ leads to weaker shocks.

Beyond the uncertainties imposed by the inability to fix fundamental nuclear parameters, such as the nuclear incompressibility and the nuclear symmetry energy coefficients, additional inconsistencies have been introduced by the use of EOSs that do not fully satisfy nuclear systematics. This has been the case with the EOSs used in the aforementioned parameter studies. The recent development of a consistently parameterized EOS (Lattimer & Swesty 1991, hereafter LS) allows us to explore in more precise detail the role of the EOS in gravitational collapse.

In § 2 we briefly discuss the EOS. In § 3 we offer a few comments about nuclear parameters and systematics. In § 4 we briefly describe the radiation hydrodynamics code and the initial model. Our results are presented in § 5, while we offer conclusions in § 6.

2. THE EQUATION OF STATE

The EOS we have employed for most of our simulations is the finite temperature compressible liquid drop EOS (Lattimer & Swesty 1991), which is based on the finite temperature compressible liquid droplet model of Lattimer et al. (1985, hereafter LLPR). The LS EOS is fully adjustable in its parameters, and the variation of its parameters is constrained by nuclear systematics. In order to maintain brevity we omit the details of the LS EOS here; for details the reader is referred to LS and LLPR. In the LS EOS matter is modeled as a mixture of a single species of heavy nuclei, alpha particles, "dripped" nucleons (which exist outside of nuclei), electrons, positrons, and photons. The basis of the model is the use of an adjustable Hamiltonian density describing the kinetic and potential energy densities of nucleons plus the energy density due to the nucleon-nucleon interaction. We use this interaction to describe bulk nucleonic matter both inside and outside of nuclei. Thus interactions among dripped nucleons are automatically consistently incorporated into the model.

The portion of the Hamiltonian density reflecting the nucleon-nucleon interaction echoes the basic density dependence of Skyrme-type Hamiltonians. We thus write the internal energy density of bulk nuclear matter as

$$E_{\rm bulk}(n_n, n_p) = \frac{\hbar^2}{2m^*}(\tau_n + \tau_p) + an^2 + bn_n n_p + \frac{cn^{1+\delta}}{1 + dn^{\delta-1}}, \quad (4)$$

where n_n and n_p, are the neutron and proton number densities, $n = n_n + n_p$, and where τ_n and τ_p are the kinetic energy densities as defined in LS. The parameters a, b, c, d, and δ determine the particular nucleon-nucleon interaction. We use the desired values of the nuclear force parameters, namely the compression modulus, the bulk symmetry energy, the nuclear saturation density, and the binding energy to determine a, b, c, and δ. Note that this interaction differs from the LS interaction (see LS eq. 2.8) by the addition of the $(1 + dn^{\delta-1})^{-1}$ factor, where $d \geq 0$, in the last term. Such an interaction could possibly result from a finite range interaction (Gogny 1975; Prakash, Ainsworth, & Lattimer 1988) and was first suggested as a way to maintain causality at high densities (Bludman & Dover 1980). We emphasize that with realistic incompressibilities *the LS EOS remains causal at all densities of interest to the supernovae problem without this parameter*. We employ this factor to effectively soften the EOS at densities above nuclear density and not to maintain causality. In the limit of $d \to 0$ we recover the LS interaction. At present there is no firm nuclear constraint on d, and its choice is ad hoc. We discuss the choice of this parameter in § 5.

From this bulk Hamiltonian we construct the bulk free energy. To this we add finite nuclear-size terms from the liquid drop model to describe the surface, Coulomb, and translational free energies. Next, the total Helmholtz free energy is minimized with respect to the compositional variables in order to obtain exact chemical and pressure equilibrium equations describing matter in thermodynamic equilibrium. The equilibrium equations are solved numerically in order to obtain the values of the compositional variables. With the composition of the system in hand, the necessary thermodynamic quantities such as the pressure, chemical potentials, etc., can be calculated by taking the appropriate combinations of derivatives of the free energy as described in LS.

3. NUCLEAR SYSTEMATICS AND THE PARAMETER SETS

The bulk energy density is determined by the choice of a, b, c, and δ in equation (4), whose values are given in terms of the parameters for symmetric matter, namely, the saturation density, n_s, the binding energy of symmetric matter, B, the volume symmetry energy, S_v, and the compression modulus,

K_s. Explicitly, the relevant relations are

$$\delta = \frac{K_s + 2\alpha + dn_s^{\delta-1}(K_s - 4\alpha - 18B)}{(1 - dn_s^{\delta-1})(3\alpha + 9B)}, \quad (5)$$

$$b = \frac{\alpha(2^{2/3} - 1) - S_v}{n_s}, \quad (6)$$

$$c = n_s^{-\delta}\frac{(\alpha/3 + B)(1 + dn_s^{\delta-1})^2}{\delta - 1}, \quad (7)$$

and

$$a = \frac{\delta(\alpha + B) - 2\alpha/3 + dn_s^{\delta-1}(\alpha/3 + B)}{n_s(1 - \delta)} - b, \quad (8)$$

where $\alpha = (3\hbar^2/10m)(3\pi^2 n_s/2)^{2/3}$. To repeat, d will be treated as a free parameter.

In addition to the terms describing bulk matter, the liquid drop EOS we employ contains finite-size terms describing contributions to the nuclear mass by surface, Coulomb, and translational effects. These finite-size terms contain other nuclear parameters, but they are highly correlated with the bulk parameters. Specifically, we refer to the surface energy, which can be parameterized in terms of the surface tension for cold symmetric matter, σ_s, and the derivatives of the surface tension,

$$S_s = -4\pi r_N^2 \frac{1}{8}\frac{\partial^2\sigma_s}{\partial x^2}\bigg|_{n=n_s, x=1/2, T=0}, \quad (9)$$

$$a_s = -4\pi r_N^2 \frac{1}{2}\frac{\partial^2\sigma_s}{\partial T^2}\bigg|_{n=n_s, x=1/2, T=0}, \quad (10)$$

which define the surface symmetry energy coefficient, S_s, and the surface contribution to the nuclear specific heat parameter, a_s. The surface tension of cold symmetric matter, σ_s, and the binding energy, B, are both well constrained by nuclear mass fits. The remaining finite-size terms, the Coulomb and translational energies, do not introduce any major additional nuclear parameters.

The surface specific heat parameter, a_s, is inherently connected to the K_s parameter. This relationship can be deduced as follows. First, the critical temperature of bulk matter, which is the maximum temperature for which two-phase coexistence of bulk matter is possible, is determined by

$$\frac{\partial P}{\partial n}\bigg|_{T_c} = \frac{\partial^2 P}{\partial n^2}\bigg|_{T_c} = 0, \quad (11)$$

where P is the bulk pressure. This condition leads to the scaling relation

$$T_c \propto \sqrt{\frac{K_s}{n_s^{2/3}}}, \quad (12)$$

which, as shown in LS, is valid for Skyrme-type Hamiltonians. Second, the surface energy is temperature dependent. As the critical temperature is approached, the surface tension of bulk matter vanishes. Calculations (Lattimer & Swesty 1991) indicate that the temperature dependence of the surface tension implies that $a_s \propto T_s^{-2}$, which is proportional to K_s^{-1}. Using this dependence, one can readily see that variations in K_s will cause variations in the specific heat of matter and hence the temperature along a given adiabat. Thus the total nuclear specific heat, and hence the entropy, depend directly on the nuclear incompressibility.

Another correlation exists between the two symmetry energy coefficients, S_v and S_s. Fits to nuclear masses are unable, by themselves, to fully establish values for S_v and S_s. Estimates of the volume symmetry energy coefficient, obtained mostly from nuclear mass formula fits, are from $S_v \sim 27$ MeV to $S_v \sim 36.5$ MeV, while the concordant variation of S_s is quite large. The dependence of the surface symmetry energy coefficient on S_v is strong. This can be explained by the need to maintain, on average for a multitude of nuclei, a constant symmetry energy contribution to the mass of a nucleus despite variations in the symmetry energy contributions S_v and S_s. In the liquid droplet model (LDM), we can write the symmetry energy per baryon of a nucleus as

$$E_{\rm sym} = \left(1 - 2\frac{Z}{A}\right)^2\left(\frac{S_v}{1 + (S_s/S_v)A^{-1/3}}\right). \quad (13)$$

For a given average nucleus, where $E_{\rm sym}$, A, and Z are fixed, consider a variation of the symmetry energies about some fiducial set of values, S_{v0} and S_{s0}. Obviously, we require

$$\frac{S_v}{1 + (S_s/S_v)A^{-1/3}} = \alpha_0, \quad (14)$$

where α_0 is a constant, in order that $E_{\rm sym}$ remain unaffected. This implies that

$$S_s = \frac{A^{1/3}}{\alpha_0}(S_v^2 - \alpha_0 S_v), \quad (15)$$

i.e., that S_s varies approximately quadratically with S_v. Allowing for variations in the other nuclear parameters, such as B and σ_s (and including shell and pairing effects), complicates the relationship between S_s and S_v. However, the basic trend of equation (15) remains unchanged. We have carried out mass fits using a basic droplet model and confirmed such a correlation between S_s and S_v. It should be pointed out that Brown (1992) argues that this correlation is weakened by finite-temperature effects; we believe such effects need further investigation.

As was shown in LS, the neutron-proton chemical potential difference, $\hat{\mu} = \mu_n - \mu_p$, and thus the free proton fraction, is strongly dependent on the surface symmetry energy. Therefore, one expects that the electron capture rate for protons will be sensitive to the symmetry energy parameterization, and it is vital to model the total symmetry energy consistently. We return to this point later.

We have employed in this study the self-consistent sets of parameters described in Table 1. These parameter sets can be grouped into two categories. The first consists of three sets in which the compression modulus varies while the symmetry energy coefficients remain constant. The second group of three consists of three parameter sets in which the symmetry energy coefficients vary while the compression moduli remain constant. In the first group, the parameters are those of the Skyrme I′ parameter set, with the exception of the compression moduli and the effective masses. The effective masses are set equal to the bare masses. We denote these parameter sets by the notation Sk375, Sk220, and Sk180 to indicate compression moduli of $K_s = 375$, 220, and 180 MeV respectively. In these parameter sets we have maintained $d = 0$ in equation (4) in accordance with LS. The latter three parameter sets arise from fits to nuclear masses or giant resonance energies. These three parameter sets were chosen by virtue of their having essentially the same incompressibility ($K_s \approx 240$ MeV), while having

TABLE 1

NUCLEAR FORCE PARAMETERS FOR MODELS IN THIS WORK

PARAMETER	PARAMETER SET					
	Sk180	Sk220	Sk375	PADNFT	MMST	MSKEH
K_s (MeV)	180	220	375	234.8	240	240
S_v (MeV)	29.3	29.3	29.3	27.5	32.5	36.5
S_s (MeV)	45.8	45.8	45.8	18.4	80.84	159.03
B (MeV)	16.0	16.0	16.0	15.85	16.279	15.986
σ_s (MeV fm^{-2})	1.15	1.15	1.15	1.06	1.36	1.20
n_s (fm^{-2})	0.155	0.155	0.155	0.161	0.153	0.147

widely varying symmetry energies. We now briefly discuss the origin of each, in the order in which they appear in Table 1.

The PADNFT parameter set is drawn from the mass fits of Pearson et al. (1991) which is based on nuclear masses calculated by the extended Thomas-Fermi technique. Such techniques offer both advantages and disadvantages over the more traditional LDM mass fits. To their advantage, the Extended Thomas-Fermi (hereafter ETF), mass formulae require only nine parameters as opposed to the 25 or so parameters required for LDM mass formulae. Ostensibly, a model with only nine parameters better reflects the underlying physics than one with 25 parameters. The mass fits, however, are based on laboratory nuclei that are nearly isospin symmetric. In contrast, the nuclei one encounters in a collapsing stellar core are extremely neutron-rich. The nine parameter mass formula ought to remain more accurate as one extrapolates to the more neutron-rich nuclei encountered in astrophysical situations. Also, the ETF formalism allows microscopic corrections to the mass formula to be added in a natural and consistent fashion, as opposed to the LDM mass formulae in which corrections are simply "added on." The disadvantages are that the mass formula does not fit quite as well as the LDM models and that the ETF model tends to underbind the heavier nuclei ($A > 250$). As can be seen in Table 1, PADNFT ETF mass formula yields the symmetry energy coefficients of $S_v = 27.5$ MeV and $S_s = 18.4$ MeV. Our values for S_v and S_s were drawn from some preliminary calculations of Pearson et al. and differ slightly from the final values they published.

The MMST parameter set is based on the LDM mass formula of Möller et al. (1988). The advantages of LDM mass formulae relative to the ETF mass formulae have been discussed above. Note that the LDM model yields a slightly higher volume symmetry energy coefficient, $S_v = 32.5$ MeV, which explains the much larger surface symmetry energy coefficient, $S_s = 80.84$ MeV.

The MSKEH parameter set comes from the Myers et al. (1977) LDM model for the giant dipole resonance (GDR) observed in nuclei. The liquid droplet parameters in this model are adjusted in order to fit the position of the resonance energies as well as nuclear masses. While the fit to the GDR energies is quite good, the symmetry parameters are substantially larger than the other two sets used here. Note, however, that this parameter set does not result from an attempt solely to model nuclear masses. From Table 1 we see that $S_v = 36.5$ MeV while $S_s = 159.03$ MeV. Comparison of the symmetry energy coefficients for the PADNFT, MMST, and MSKEH parameter sets thus clearly illustrates the strong relationship between S_v and S_s.

For the purposes of comparison we have also employed the EOS of Cooperstein & Baron (1990, hereafter CB) which incorporates the supernuclear parameterization of BCK). This EOS, though adjustable in its parameters, is not necessarily fully consistent with nuclear systematics. Most notably, the parameterization of the nuclear symmetry energy does not allow for separate surface and volume symmetry energy coefficients.

An important constraint that all EOSs should meet is the neutron star mass constraint imposed by the observationally measured properties of the binary pulsar system PSR 1913+16 (Weisberg & Taylor 1984). The larger of the two neutron stars in this system has a mass of 1.44 $M_\odot$; thus, the cold beta-equilibrium EOS should result in a maximum neutron star mass of at least this value. Additionally, the EOS should remain causal at all densities found in both neutron stars and supernovae. We have constructed neutron star models by numerically solving the Tolman-Oppenheimer-Volkoff equations with the four extrema of our parameter sets: K375, K180, MS, PADNFT. For the ease of numerical computation, we have used the subnuclear EOS of Baym, Pethick, & Sutherland (1971, hereafter BPS) for all of the hydrostatic models we have built. The fraction of the neutron star mass originating from matter at subnuclear densities is insignificant, and the choice of the EOS in this regime is of little consequence to the maximum mass. The resulting mass versus central density curves are presented in Figure 1. We have also presented the mass as a function of central density curve for the BCK EOS with the parameters often chosen for supernova simulations ($K_s = 180$ MeV, $\gamma = 2.5$). We wish to emphasize that although the BCK

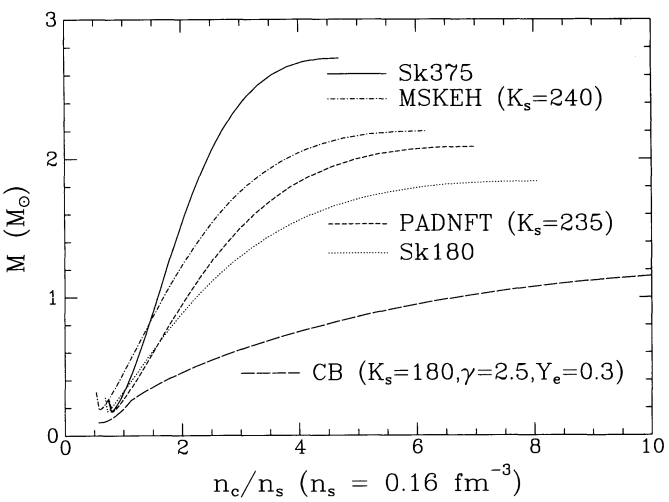

FIG. 1.—Neutron star mass vs. central density (in units of nuclear saturation density) for the three different compression moduli.

EOS is fully capable of describing the matter in a neutron star of mass greater than 1.44 $M_\odot$ with many parameter sets, the parameter sets often used in supernova simulations result in an EOS that is incapable of meeting the observational lower limit imposed by PSR 1913+16. The failure to meet this constraint has very important consequences for the prompt explosion mechanism.

4. THE RADIATION HYDRODYNAMIC MODEL

The work presented here was carried out using a modified version of the one-dimensional radiation hydrodynamic code described in Myra et al. (1987), hereafter MBHLSV) and MB. The code, which we have named BRYTSTAR, has been modified to use the LS EOS. The hydrodynamical evolution of the iron core is solved using the one-dimensional general relativistic hydrodynamics equations in Lagrangean coordinates. The equations are solved by finite-difference techniques using the modified Lagrange form of the Richtmyer & Morton (1967) artificial viscosity as implemented by Noh (1987). In practice we have used 60 spatial zones, with the zoning weighted toward the edge of the core. While such zoning may be too coarse for detailed late-time calculations, it is more than sufficient to allow a comparison between various equations of state during the infall and bounce stages.

The neutrino transport is described by the general relativistic radiation energy equation, which we close at the level of the first moment by means of the Levermore & Pomraning (1981) flux limiter scheme. The solution of the equations is then accomplished by finite-differencing them in a Lagrangean mass coordinate and in the neutrino energy and then solving them by a method based on an n-precursor scheme developed by N. Sack (see MBHLSV). We have employed 25 energy groups along with the same 60 spatial zones used for the hydrodynamics differencing. Although we are primarily interested in a comparison of results among various EOSs, we conducted a convergence test for our code. In order to see if the shock dynamics was affected by the number of mass zones, we doubled the zoning in mass. We have found no notable differences between the 120 and 60 zone cases in the density profile at bounce, the location of the shock stall point (in either radius or mass), etc., within the limit of the resolution. Plots of this data show nearly identical results between the two cases and have not been included here.

It is important to have a sufficient number of energy groups in order to fully resolve the Fermi surface of the neutrino distribution. As was pointed out in MBHLSV, resolution of the Fermi surface of the degenerate neutrinos is vital in order to accurately model the radiation-matter energy exchange. For this reason, we have insisted on having a relatively large number of groups in our simulations. The grouping scheme is geometrical in nature; the width of each group is the width of the next lower energy group multiplied by a scale factor. The width of the lowest group is approximately 2.5 MeV. The scale factor monotonically decreases from approximately 1.18 for the lowest energy groups to 1.05 for the highest energy groups. Our experience has shown that the highest energy group, which is centered at approximately 200 MeV, has little or no occupancy over the course of our calculations.

All the standard neutrino processes described in MBHLSV and in MB have been included, with the exception of electron capture onto heavy nuclei. The overall capture rate is dominated by capture of electrons onto free protons. In addition, the presence of heavy nuclei influence the depletonization only for nuclei where $N < 40$ (Fuller 1982). The use of an $N > 40$ electron capture cutoff for heavy nuclei is somewhat suspect when combined with a single-nucleus EOS, and we thus neglect it. We have included neutrino-electron scattering in the Fokker-Planck approximation of Bowers & Wilson (1982) as described in MBHLSV.

The progenitor is the $\sim 1.2\ M_\odot$ core of the 13 $M_\odot$ model of Nomoto & Hashimoto (1988). We do not have any particular affinity for this progenitor model; rather, we have employed it for these calculations in order to facilitate comparisons to previous work. Because the EOS used by Nomoto & Hashimoto differs from ours, we have chosen to maintain the temperature, density, electron fraction, and velocity from their progenitor model as we convert to our EOS. Since the electron contribution to the EOS is well-known and dominates the pressure, the pressure is essentially maintained also.

5. PROMPT TIMESCALE COLLAPSE SIMULATIONS

The results of our BRYTSTAR simulations are presented in Figures 2–8. We begin first by an analysis of our results concerning the role of the nuclear incompressibility.

It has long been assumed that the incompressibility plays a strong role in determining the dynamics of shock propagation in the collapse and bounce phases of Type II supernovae. The hypothesis is that a softer EOS allows the shock to propagate further outward before either stalling or reaching the edge of the iron core. However, when we employ EOSs constrained by PSR 1913+16, we find (Figs. 2*a*–2*c*) no evidence to support this hypothesis. These radius versus time plots, in which the radius at a given enclosed mass is plotted against time, show clearly that there is no discernible difference in the shock stall radius among the Sk180, Sk220, and Sk375 cases.

In contrast, the results are radically different when the CB EOS is employed. Figure 3 shows the time evolution of the same initial model using the CB EOS. Note that the shock stall radius is approximately 3 times larger than any of the LS EOS cases. This surprising difference in the shock dynamics is essentially because the CB EOS with the standard parameter set is substantially softer than any of the LS EOS cases (see Fig. 10 of LS). Such behavior was first noted in stellar collapse using a polytropic EOS by Van Riper (1978). However, the softness of the CB EOS with $K_s = 180$ MeV and $\gamma = 2.5$ violates the PSR 1913+16 constraint.

In order to ascertain whether or not the shock dynamics obtained with the LS EOS could be affected by substantially softening the EOS, we performed more simulations in which we adjusted the d parameter in our Skyrme-line interaction potential to just meet the 1.44 $M_\odot$ PSR 1913+16 limit. The Sk180 and Sk375 parameter sets with the additional nonzero d parameter are designated as Sk180* and Sk375*. Figure 4 illustrates the maximum mass versus central density plots for the modified and unmodified EOSs. Despite the additional softening, the shock dynamics on prompt timescales is unaffected: shocks continue to stall near 100 km. We have not bothered to include a Lagrangean mass plot for this case as the results show little quantitative difference from the cases shown in Figures 2*a*–2*c*. We conclude that if the EOS is stiff enough to meet the PSR 1913+16 constraint, the variation of nuclear incompressibility has no noticeable effect on the prompt shock dynamics.

Next, we examine the neutrino luminosities from the three LS "Skyrme" models and the CB EOS, which are shown in Figures 5*a*–5*c* and Figure 6. The very small scale structure

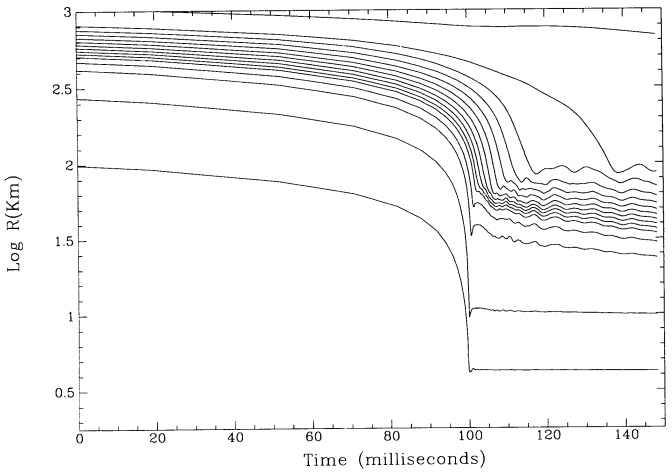

FIG. 2a

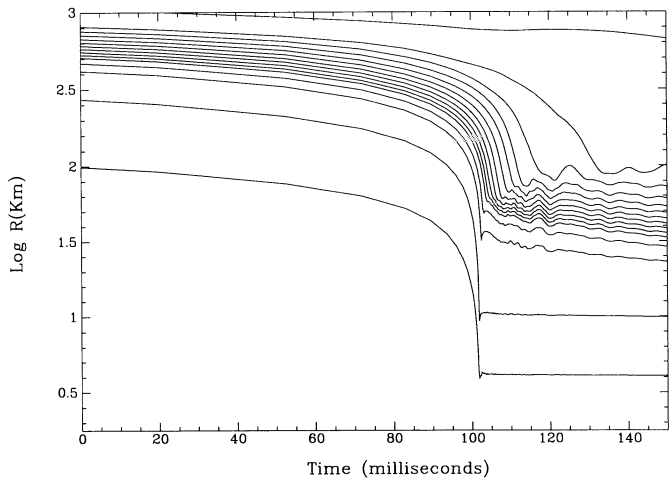

FIG. 2c

FIG. 2.—(*a*) Log of the radius of a given mass shell (in kilometers) vs. time (in units of milliseconds) for the run using the Sk375 parameter set. (*b*) Log of the radius of a given mass shell (in kilometers) vs. time (in units of milliseconds) for the run using the Sk220 parameter set. (*c*) Log of the radius of a given mass shell (in kilometers) vs. time (in units of milliseconds) for the run using the Sk180 parameter set.

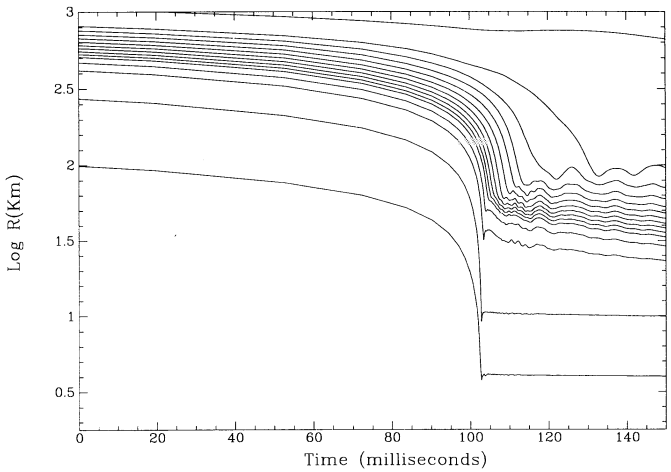

FIG. 2b

(glitches) in the luminosities following the peak corresponding to shock breakout is numerical in origin and does not affect the overall neutrino energy radiation rate. There are no substantial differences among the three LS EOS cases. The electron neutrino luminosity does increase with K_s, which is a result of the inverse relationship between K_s and the specific heat as illustrated in § 3. With increasing K_s, the temperature along an adiabat increases and forces the dripped proton fraction to increase. It is this increase in the proton fraction and the consequent rise in the electron capture rate that causes the electron neutrino luminosity to increase with K_s. The increased electron capture rate also contributes to the softening of the EOS by removing part of the pressure support provided by the electrons and allows the collapse to proceed faster. This explains why the bounce occurs a few milliseconds faster in the stiffer EOS cases than it does in the softer models. One should note (see Table 2) that the central density at bounce increases as the EOS gets softer. Especially note the substantially higher central densities achieved with the CB EOS. The high density achieved at bounce is responsible for the peak in the muon neutrino luminosity at shock breakout seen in Figure 6. This peak, which was discussed in Myra & Burrows (1990), is a

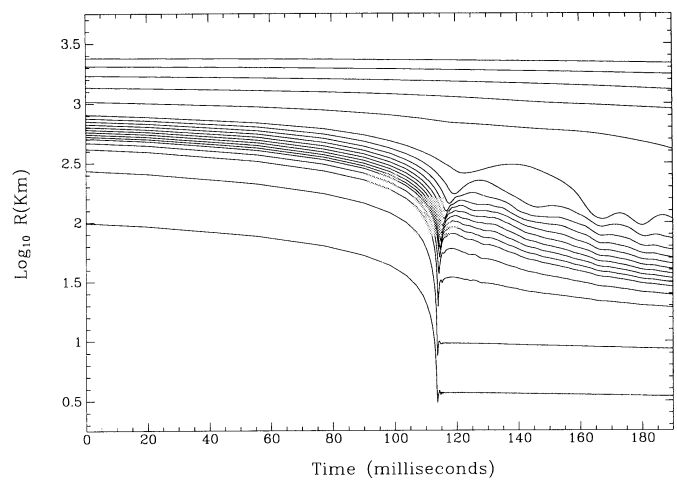

FIG. 3.—Log of the radius of a given mass shell (in kilometers) vs. time (in units of milliseconds) for the run using the CB EOS with $K_s = 180$ MeV and $\gamma = 2.5$.

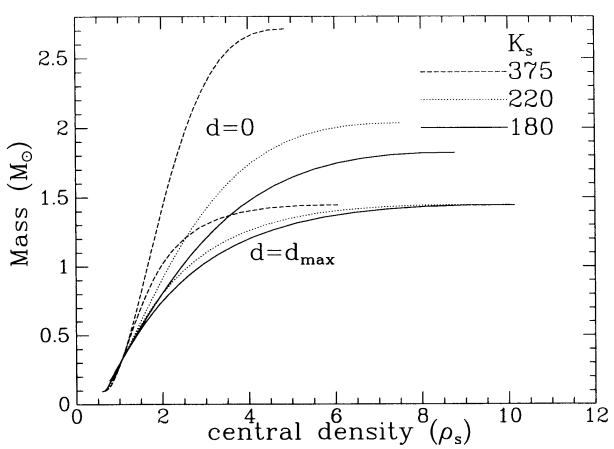

FIG. 4.—Neutron star mass vs. central density (in units of nuclear saturation density) for the Sk375, Sk220, and Sk180 cases with $d = 0$ and $d = d_{max}$, the value of d that produces a maximum neutron star mass of 1.44 $M_\odot$.

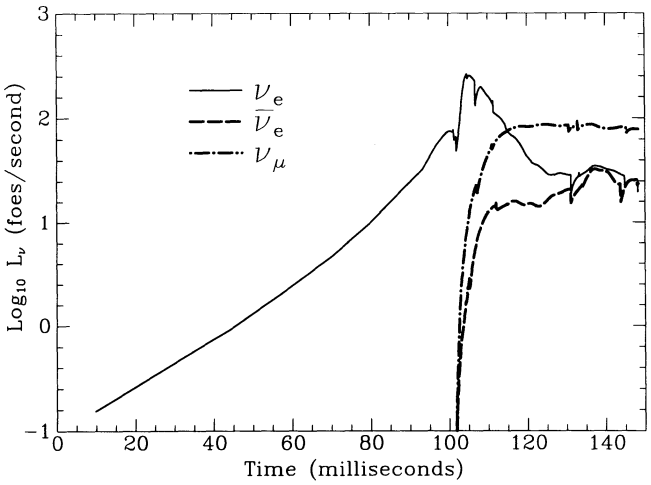

FIG. 5a

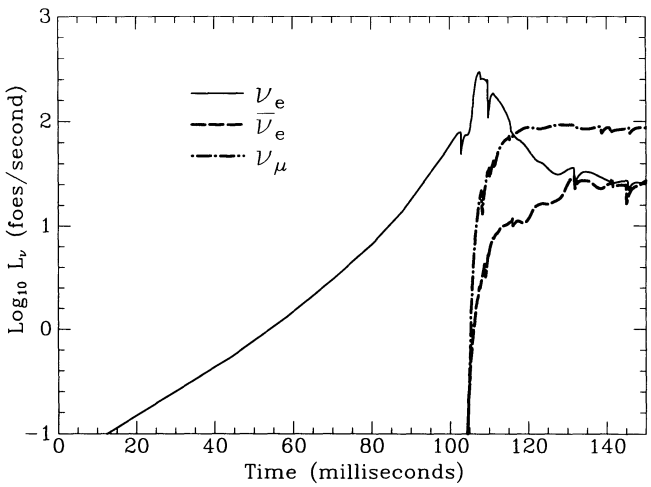

FIG. 5c

FIG. 5.—(*a*) Log of the neutrino luminosities (in foes s^{-1}; 1 foe = 10^{51} ergs) vs. time for the run using the Sk375 parameter set. (*b*) Log of the neutrino luminosities (in foes s^{-1}; 1 foe = 10^{51} ergs) vs. time for the run using the Sk220 parameter set. (*c*) Log of the neutrino luminosities (in foes s^{-1}; 1 foe = 10^{51} ergs) vs. time for the run using the Sk180 parameter set.

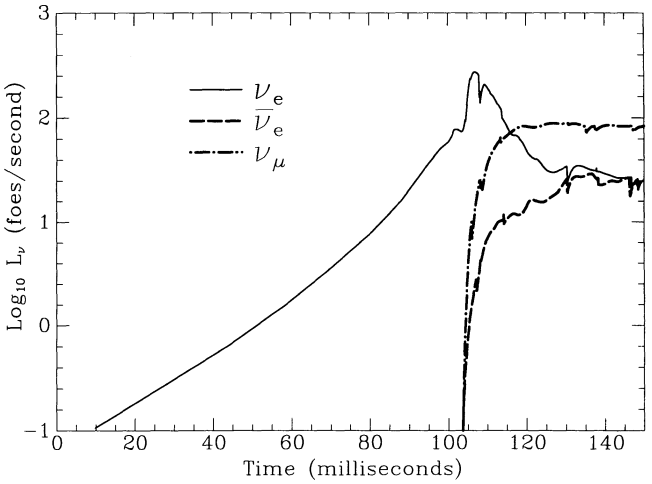

FIG. 5b

result of the pair production from the strong shock formed with the CB EOS.

The CB EOS also has a substantially lower specific heat than the LS EOS (see Fig. 8 of LS) above nuclear densities. The lower specific heat combined with the higher bounce density radically affects the temperature profile in the core in the post-bounce epoch. This is readily seen from Figure 7 where the temperature profiles for the Sk180, Sk220, Sk375, and CB cases are displayed. Note that the temperature *increases* outward from the center to the stalled shock for the LS cases, while it *decreases* in the same region for the CB EOS. The contrast in the central temperatures at bounce is quite striking with a 15 MeV temperature for the LS EOS cases and a 25 MeV temperature for the CB EOS. This difference in temperature profiles is a result of the large difference in central densities at bounce. (The assumption that $m^* = m$ that is employed in the LS EOS slightly overestimates the specific heat of matter. Because the stellar collapse models in which we have used the LS EOS do not achieve high densities, this has little effect on the actual temperature.)

We turn now to a discussion of varying the symmetry energy parameterization. Consider the three symmetry energy param-

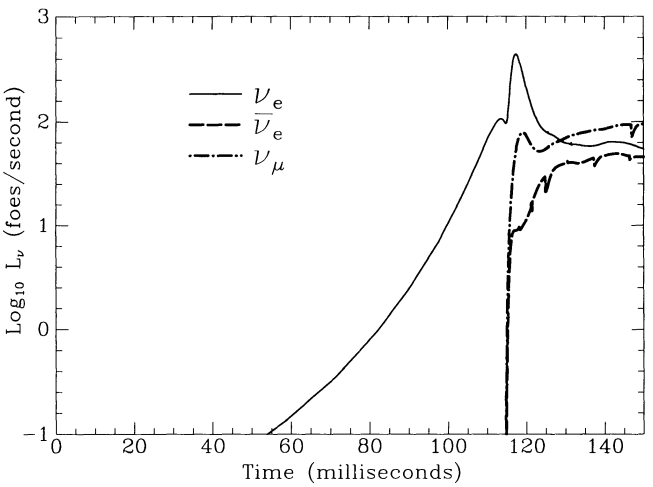

FIG. 6.—Log of the neutrino luminosities (in foes s^{-1}; 1 foe = 10^{51} ergs) vs. time for the run using the CB EOS with K_s = 180 MeV and γ = 2.5.

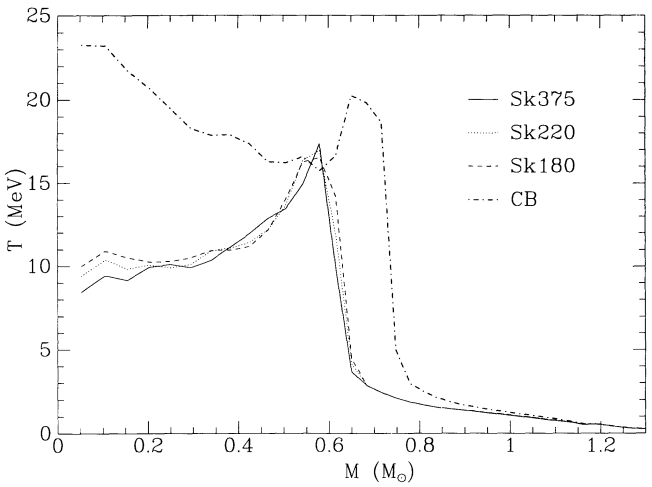

FIG. 7.—Temperature profiles at bounce for the cases Sk375, Sk220, Sk180, and CB.

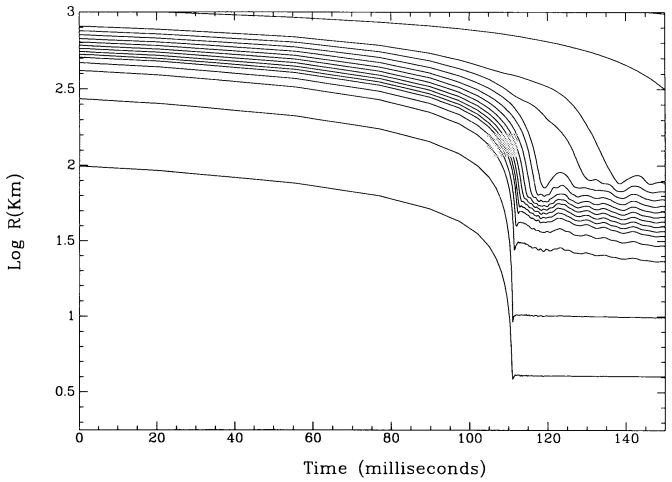

FIG. 8*a*

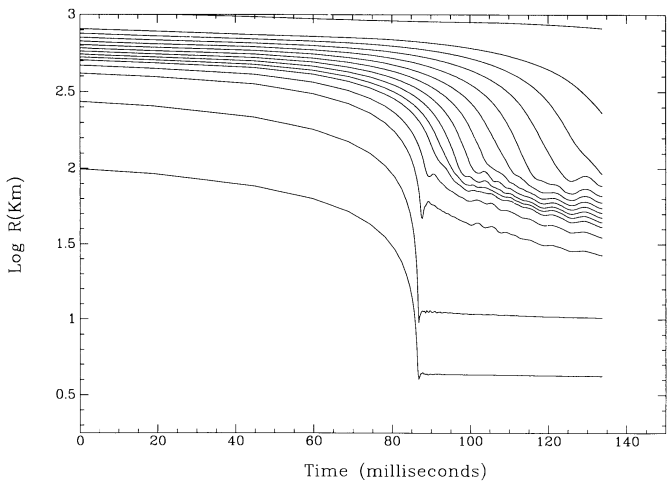

FIG. 8*c*

FIG. 8.—(*a*) Log of the radius of a given mass shell (in kilometers) vs. time (in units of milliseconds) for the run using the PADNFT parameter set. (*b*) Log of the radius of a given mass shell (in kilometers) vs. time (in units of milliseconds) for the run using the MMST parameter set. (*c*) Log of the radius of a given mass shell (in kilometers) vs. time (in units of milliseconds) for the run using the MSKEH parameter set.

eter sets: PADNFT, MMST, and MSKEH, where the results are shown in Figures 8*a*–8*c*. The shock stall radius is again largely constant among the three cases, with a stall radius of about 100 km as in the previously discussed incompressibility cases. However, the lower symmetry energy cases do permit the shock to propagate out through slightly more of the iron core ($\sim 0.1\ M_\odot$) due to the decrease in deleptonization with

TABLE 2

CENTRAL DENSITY AT BOUNCE

Parameter Set	$\rho_{\rm bounce}$	n/n_s
PADNFT ($S_v = 27.5$)	4.35×10^{14}	1.620
MMST ($S_v = 32.5$)	3.89×10^{14}	1.525
MSKEH ($S_v = 36.5$)	3.83×10^{14}	1.563
K375	3.56×10^{14}	1.378
K220	4.24×10^{14}	1.638
K180	4.62×10^{14}	1.785
CB ($K = 180, \gamma = 2.5$)	9.01×10^{14}	3.378

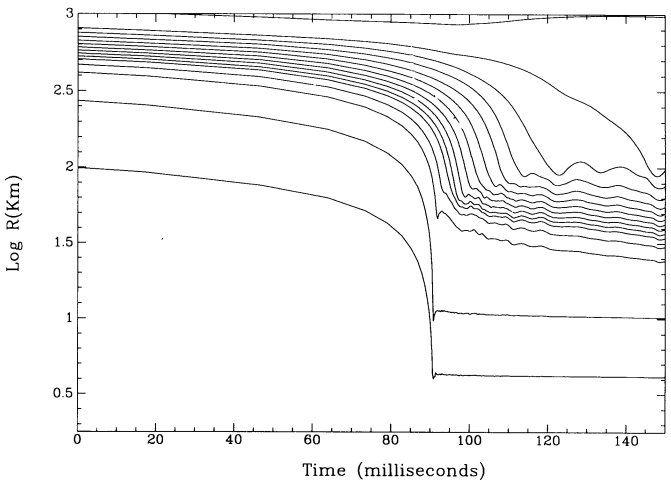

FIG. 8*b*

decreasing volume symmetry energy coefficient, which we discuss below. There is a wider variation among these cases in the time it takes the collapsing core to reach bounce than among the varying-incompressibility cases. The bounce in the MSKEH case occurs approximately 24 ms sooner than bounce with the PADNFT parameters. This effect is due to the increased electron capture rate caused by variation of the symmetry energy coefficients. The higher electron capture rate more rapidly reduces the density of electrons, which provide the dominant contribution to the pressure, and creates a larger pressure deficit during the collapse. This high rate of electron capture is evidenced also in Figure 9*c*, where the electron neutrino luminosity prior to bounce is much higher in the MSKEH case than in either the MMST or PADNFT cases.

From Figures 9*a*–9*c* we can see that the electron neutrino luminosity, and hence the electron capture rate, increases with the volume symmetry energy. This result is *opposite* that of Bruenn (1989) who found, using the CB EOS, that the electron capture rate decreases with increasing volume symmetry energy. This discrepancy results from the neglect of the variation of the surface symmetry energy coefficient in the CB EOS. In a simple liquid drop analysis, the difference in neutron and proton chemical potentials is approximately given by

$$\hat{\mu} = \mu_n - \mu_p \approx 8(S_v - A^{-1/3}S_s)\left(\frac{1}{2} - \frac{Z}{A}\right). \qquad (16)$$

Note that S_s enters into equation (16) with sign opposite to that of S_v. Because of the strong correlation between the volume and surface symmetry energy parameters, as the volume symmetry coefficient is increased, the value of $\hat{\mu}$ actually decreases; the relative effect of the surface term outweighs that of the volume term. For matter during the collapse phase, before the onset of nucleon degeneracy, which is usually the case before neutrino trapping occurs, the neutron to proton ratio is given by

$$\frac{n_p}{n_n} = e^{-\hat{\mu}/T}. \qquad (17)$$

Thus a larger value of S_v increases the number of protons available for capture if the correlation of S_v and S_s is considered.

If one neglects the surface symmetry energy term, as does the CB EOS, the $\hat{\mu}$ instead decreases with increasing S_v, and thus

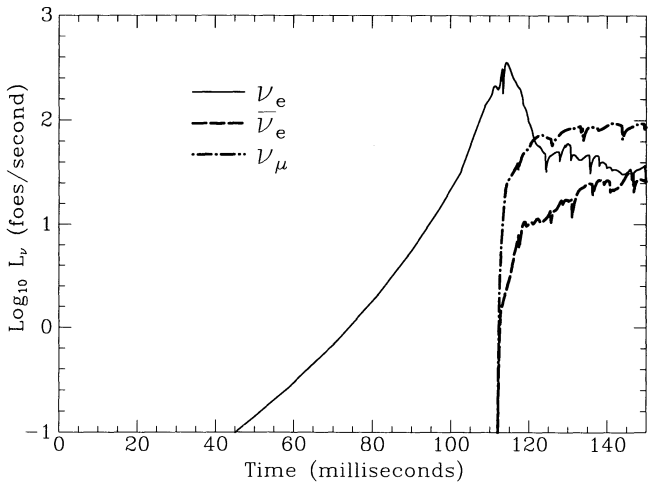

FIG. 9a

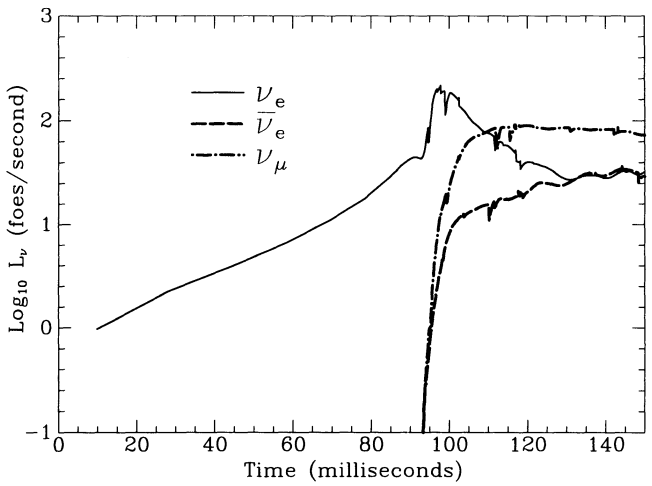

FIG. 9b

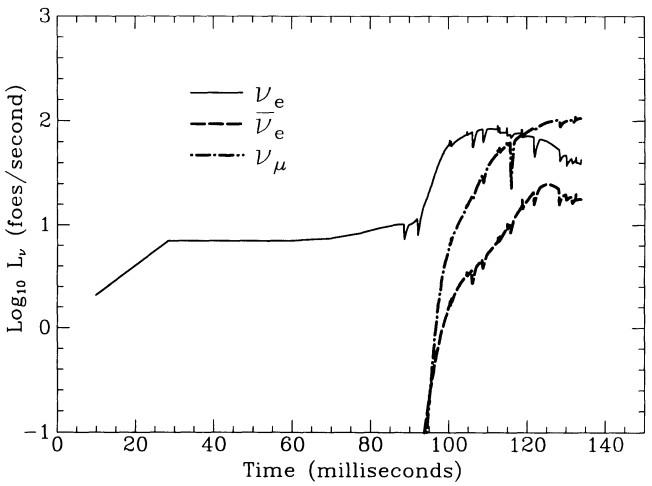

FIG. 9c

FIG. 9.—(*a*) Log of the neutrino luminosities (in foes s^{-1}; 1 foe = 10^{51} ergs) vs. time for the run using the PADNFT parameter set. (*b*) Log of the neutrino luminosities (in foes s^{-1}; 1 foe = 10^{51} ergs) vs. time for the run using the MMST parameter set. (*c*) Log of the neutrino luminosities (in foes s^{-1}; 1 foe = 10^{51} ergs) vs. time for the run using the MSKEH parameter set.

the amount of electron capture decreases. The neglect of the surface term is only justified if $S_v \gg A^{-1/3}S_s$: a situation that never occurs for typical values of A and S_s.

It is of interest that the CB electron neutrino luminosity during infall is comparable to the PADNFT case. However, the CB EOS employs a 31.5 MeV volume symmetry energy coefficient, while the PADNFT case has $S_v = 27.5$ MeV. This again illustrates the necessity of separately parameterizing the surface symmetry energy. To simply vary the volume symmetry energy coefficient by itself is not consistent with nuclear systematics and can substantially affect the electron neutrino luminosity.

The most remarkable difference between the three symmetry energy cases is in the neutrino luminosities themselves. The luminosity is much more sharply peaked in the PADNFT case, corresponding to a relatively late occurrence of electron capture and a relatively large homologous core. In the extreme MSKEH case, the peak is much more spread out. This is mainly due to the greater depth in the core at which the shock has formed. Also note that in the PADNFT and MMST models the electron neutrino and electron antineutrino curves have more or less merged by about 30 ms after bounce. This merging indicates the onset of detailed balance in the electron capture and proton capture that produce each of these species. However, in the MSKEH case the curves are still substantially separated 30 ms after bounce. This is because the rates are not in detailed balance; the collapse has proceeded so rapidly that the neutrino trapping has overwhelmed the increased electron capture rates. Whether or not these differences could be observed in a large neutrino experiment such as Super-Kamiokande or the Sudbury Neutrino Observatory is a subject that we currently are investigating.

6. CONCLUSIONS

We have found a number of interesting results regarding the role of the EOS in stellar collapse on prompt timescales. First, the cherished belief that the nuclear incompressibility determines the shock dynamics is unfounded when one incorporates the 1.44 $M_\odot$ neutron star constraint imposed by observations of the binary neutron star system PSR 1913+16. Only if the EOS is softened to a degree that is unphysical could the prompt shock dynamics change appreciably. In order for the shock to propagate promptly to a larger radius the EOS must be very soft at densities just above nuclear densities, which seems to be inconsistent with the 1.44 $M_\odot$ constraint. Surprisingly, we have found virtually no change in the shock stall radius as both the compression modulus and the symmetry energy coefficients are varied over wide ranges. However, the variation of the symmetry energy coefficients causes variations in the rate of electron capture. This produces changes in the neutrino luminosities, which are potentially observable. This does not produce a strong change in the trapped lepton fraction in the era just after core bounce. We reiterate, however, that the parameterization of the symmetry energy and the variation of the symmetry energy coefficients *must* be performed in a fashion consistent with nuclear systematics. Finally, while we have been able to offer some definitive statements about the role of the EOS in the prompt phase of core collapse supernovae, we are as yet unable to make the analogous statements about the role of the EOS and the late-time mechanism. We are currently extending these investigations of the role of the EOS to the late-time epoch.

We would like to thank Jerry Cooperstein and Edward Baron for providing us with the CB EOS and for their helpful criticism. We would like to thank Steve Bruenn, Adam Burrows, and Ken Van Riper for many useful discussions and the referees for helpful suggestions. We wish to acknowledge computing support from the Pittsburgh Supercomputing Center and the National Energy Research Supercomputing Center and financial support under DOE grant DE-FG02-87ER40317.

REFERENCES

Baron, E. A., Cooperstein, J., & Kahana, S. 1985a, Phys, Rev. Lett., 55, 126
———. 1985b, Nucl. Phys. A, 440, 744
Baron, E., Bethe, H. A., Brown, G. E., Cooperstein, J., & Kahana, S. 1987, Phys. Rev. Lett., 59, 736
Baym, G., Pethick, C., & Sutherland, P. 1971, ApJ, 170, 299
Bludman, S. A., & Dover, C. B. 1980, Phys. Rev. D, 22, 1333
Bowers, R. L., & Wilson, J. R. 1982, ApJS, 50, 115
Brown, G. E. 1993, in Proc. 1st Symp. on Nuclear Physics in the Universe, ed. M. Guidry (Bristol: Adam Hilger), 65
Bruenn, S. W. 1989a, ApJ, 340, 955
———. 1989b, ApJ, 341, 385
Cooperstein, J., & Baron, E. A. 1990, in Supernovae, ed. A. Petschek (New York: Springer-Verlag), 213
Fuller, G. M. 1982, ApJ, 252, 741
Gogny, D. 1975, in Nuclear Self-Consistent Fields, ed. G. Ripkaand & M. Porneuf (Amsterdam: North-Holland), 333
Lattimer, J. M., Burrows, A. S., & Yahill, A. 1985, ApJ, 288, 644
Lattimer, J. M., Pethick, C. J., Ravenhall, D. G., & Lamb, D. Q. 1985, Nucl. Phys. A, 432, 646
Lattimer, J. M., & Swesty, F. D. 1991, Nucl. Phys. A, 535, 331
Levermore, C. D., & Pomraning, G. C. 1981, ApJ, 248, 321
Ludwig, S., Von Groote, H., Hilf, E., Cameron, A. G. W., & Truran, J. 1973, Nucl. Phys. A, 203, 627
Miralles, J. A., Ibanez, J. M., Martis, J. M., & Perez, A. 1991, A&AS, 90, 283
Möller, P., Meyers, W., Swiatecki, W. J., & Treiner, J. 1988, Atomic Data Nucl. Data Tables, 39, 225
Myers, W., Swiatecki, W. J., Kodama, T., El-Jaick, L. J., & Hilf, E. R. 1977, Phys. Rev. C, 15, 2032
Myra, E. S., & Bludman S. A. 1989, ApJ, 340, 384
Myra, E. S., Bludman, S. A., Hoffman, Y., Lichtenstadt, I., Sack, N., & Van Riper, K. A. 1987, ApJ, 318, 744
Myra, E. S., & Burrows, A. 1990, ApJ, 364, 222
Noh, W. F. 1987, J. Comput. Phys., 72, 78
Nomoto, K., & Hashimoto, M. 1988, Phys. Rep., 163, 13
Pearson, J. M., Aboussir, Y., Dutta, A. K., Nayak, R. C., Farine, M., & Tondeur, F. 1991, Nucl. Phys. A, 528, 1
Prakash, M., Ainsworth, T. L., & Lattimer, J. M. 1988, Phys, Rev. Lett., 61, 2518
Richtmeyer, R. D., & Morton, K. W. 1967, Difference Methods for Initial Value Problems (2nd ed.; New York: Interscience)
Van Riper, K. A. 1978, ApJ, 221, 304
———. 1979, ApJ, 232, 558
Weisberg, J. M., & Taylor, J. H. 1984, Phys. Rev. Lett., 52, 1348